Characterization of worn Ti-Si cathodes used for reactive cathodic arc evaporation

Jianqiang Zhu, Anders Eriksson, Naureen Ghafoor, M P Johansson, J Sjolen, Lars Hultman, Johanna Rosén and Magnus Odén

Original Publication:

Jianqiang Zhu, Anders Eriksson, Naureen Ghafoor, M P Johansson, J Sjolen, Lars Hultman, Johanna Rosén and Magnus Odén, Characterization of worn Ti-Si cathodes used for reactive cathodic arc evaporation, 2010, JOURNAL OF VACUUM SCIENCE and TECHNOLOGY A, (28), 2, 347-353.
http://dx.doi.org/10.1116/1.3330767

Characterization of Worn Ti-Si Cathodes Used for Reactive Cathodic Arc Evaporation

J.Q. Zhu[1*], A. Eriksson[2], N. Ghafoor[1], M. P. Johansson[3], J. Sjölén[3], L. Hultman[2], J. Rosén[2], M. Odén[1]

1. Nanostructured materials, Department of Physics, Chemistry, and Biology (IFM), Linköping University, SE-581 83 Linköping, Sweden

2. Thin Film Physics, Department of Physics, Chemistry, and Biology (IFM), Linköping University, SE-581 83 Linköping, Sweden

3. SECO Tools AB, SE-737 82 Fagersta, Sweden

Abstract

The microstructural evolution of $Ti_{1-x}Si_x$ cathode surfaces (x=0, 0.1, 0.2) used in reactive cathodic arc evaporation has been investigated by analytical electron microscopy and x-ray diffractometry. The results show that the reactive arc operated in N_2 atmosphere induces a 2-12 μm thick N-containing converted layer consisting of nanosized grains in the two-phase Ti and Ti_5Si_3 cathode surface. The formation mechanism of this layer is proposed to be surface nitriding and redeposition of macroparticles formed during the deposition process. The surface roughness of the worn $Ti_{1-x}Si_x$ cathodes increases with increasing Si content, up to 20 at%, due to preferential erosion of Ti_5Si_3.

Keywords

Reactive cathodic arc evaporation, cathode surface, preferential erosion, nitriding.

* Corresponding author: zhu@ifm.liu.se

I. Introduction

Cathodic arc evaporation (CAE) is a commonly used physical vapor deposition technique for hard coatings, e.g., as wear resistant coatings on cutting tools. In general, cathodes are fabricated from sufficiently conductive materials, such as pure metal or metal alloys. In the case of hard coatings, pure Ti was initially employed to produce TiN coatings in the early 1970s [1]. Ti alloys are subsequently used to deposit TiN-based ternaries, such as TiAlN [2-7], and more recently quarternary coatings, such as TiAlSiN [8]. It is widely acknowledged that when evaporating from a pure metal cathode in a reactive N_2 atmosphere, a compound layer forms on the surface of the cathode, which can significantly influence the deposition process [9-15]. However, the nature of this compound layer has not been characterized beyond establishing the presence of N in the surface.

For reactive CAE, Boxman et al. [15] suggested that the nitriding effect of a Ti cathode surface when operated in a N_2 atmosphere results in less metal ions in the plasma and a different erosion rate compared with a pure Ti surface. Coll et al. [16] proposed an empirical model for the so called "poisoning effect" of nitrogen based on reaction kinetics and energy balance, and qualitatively discussed how it influences the CAE process conditions in terms of the evaporation rate, deposition rate and formation of macroparticles (also known as droplets). Similarly, Kim et al. [14] attributed the reduced erosion rate to the presence of TiN on the cathode surface. Aksenov [17] and Kühn [18] qualitatively confirmed the presence of nitrogen on Ti cathode surface by XPS and RBS, respectively. Hovsepian et al. [19] studied the degree

of cathode poisoning and suggested that the observed reduced erosion rate in a reactive N_2 CAE process is related to the formation of Ti_2N and TiN on the cathode surface. Thus, in the aforementioned work of CAE from pure Ti cathodes, an agreement exists that the erosion rate is reduced in a reactive N_2 atmosphere, attributed to an alleged compound layer formed on the cathode surface.

Currently, compound or alloyed cathodes (e.g. Ti-Al, Ti-Si etc.) are frequently used in industrial reactive CAE processes of Ti-containing multi-component coatings, which have superior properties compared to TiN. For example, Ti-Al-N [2-7] and Ti-Si-N [20-21] coating systems have gained interest because of their much improved mechanical properties and high thermal stability compared to TiN [22-24]. In Ti-Si-N ternary system, there is no stable ternary Ti-Si-N compound [25], but several Ti-N, Si-N, and Ti-Si binaries. Hence, the nitriding effect of a Ti-Si cathode, i.e., the formation of a converted layer (we name it converted layer in our work to distinguish it from the cases when the cathode itself is a compound) during a reactive CAE process, will yield a multiphase microstructure. Since each phase has its own evaporation characteristics, it is expected that the very formation of a converted layer will influence the as-deposited coating composition, microstructure and properties. However, no report referring to the surface evolution of Ti-Si alloyed cathode and its influence on the reactive CAE process has been found.

The present work concerns the evolution of microstructure and composition of $Ti_{1-x}Si_x$ (x=0, 0.1 and 0.2) alloy cathode surfaces during a reactive arc process. The samples cut from the cathode surfaces were investigated by x-ray diffractometry

(XRD), scanning electron microscopy (SEM) and analytical transmission electron microscopy (ATEM), wherein focused ion beam milling (FIB) was used to prepare TEM cross-sectional samples. The results show that the N_2 reactive arc process induces a converted layer covering the cathode surface, which differs in microstructure and composition from the virgin material. A model for the formation of this converted layer is also presented.

II. Experimental

Powder metallurgical $Ti_{1-x}Si_x$ (x=0, 0.1, and 0.2) cathodes were used to produce Ti-Si-N coatings with a commercial Metaplas Compact arc evaporation system [6]. The 26 mm thick disc-shaped cathodes, 63 mm in diameter, were run with an arc current of 50 A in a pure N_2 atmosphere for more than 10 h (8 times × 80 min/time) to ensure steady state conditions. During evaporation, the cathodes were water cooled through a Cu-plate back support. Afterwards, specimens approximately 20×20×5 mm^3 were cut from the surfaces of worn cathodes for further characterization.

X-ray diffraction was carried out on a PANalytical X'pert Pro MRD system (Philips, Netherlands), using Cu Kα radiation. The diffractograms were recorded with a grazing incidence angle of 4º. Surface roughness was measured by a TalySurf PGI840 profilometer (Taylor-Hobson, UK). The microstructure and surface chemistry were investigated with a LEO 1550 SEM (Zeiss, Germany) equipped with an INCA energy dispersive x-ray spectrometer (EDX) (Oxford, UK) and operated at 5 kV in image mode and at 20 kV during elemental mapping. Cross-sectional thin foils of the

converted layer for TEM were prepared by FIB using a 1540 EsB cross beam instrument (Zeiss, Germany). Details of cross-sectional TEM specimen preparation are given elsewhere [26]. In order to acquire sufficiently thin sample for transmission electron microscopy, the samples were further thinned by a RES 010 ion beam miller (BAL-TEC, Switzerland). Microstructural analysis of the surface converted layer was carried out with a Tecnai G^2 TF 20 UT FEG TEM operated at 200 kV (FEI, Netherlands). Scanning transmission electron microscopy (STEM) micrographs was recorded using a high-angle annular dark-field (HAADF) detector with variable camera length. Compositional analysis in STEM mode was conducted by EDX and electron energy loss spectroscopy (EELS).

III. Results

A. General features of the $Ti_{1-x}Si_x$ cathodes

Figure 1 shows the diffractograms of (a) the virgin and (b) the worn cathode surfaces for x = 0, x = 0.10, and x = 0.20, respectively. For the virgin material (Figure 1a), only the α-Ti phase was observed for the pure Ti cathode (x = 0) whereas both the Ti_5Si_3 phase and the solid solution α-Ti(Si) phase were found in the alloyed cathodes (x = 0.10 and x = 0.20). The amount of Ti_5Si_3 phase increased with increasing Si content of the cathodes. After operating the cathodes in a reactive N_2 atmosphere, the cubic TiN phase appears on the surfaces in addition to the phases observed in the virgin material (see Figure 1b). Besides TiN, small amounts of SiN_y ($y \approx 4/3$) forms on the alloyed cathodes ($Ti_{90}Si_{10}$ and $Ti_{80}Si_{20}$). Moreover, the full width

half maximum (FWHM) of the peaks from the worn cathodes are broader indicating a reduction of the grain size compared to that of the virgin cathodes.

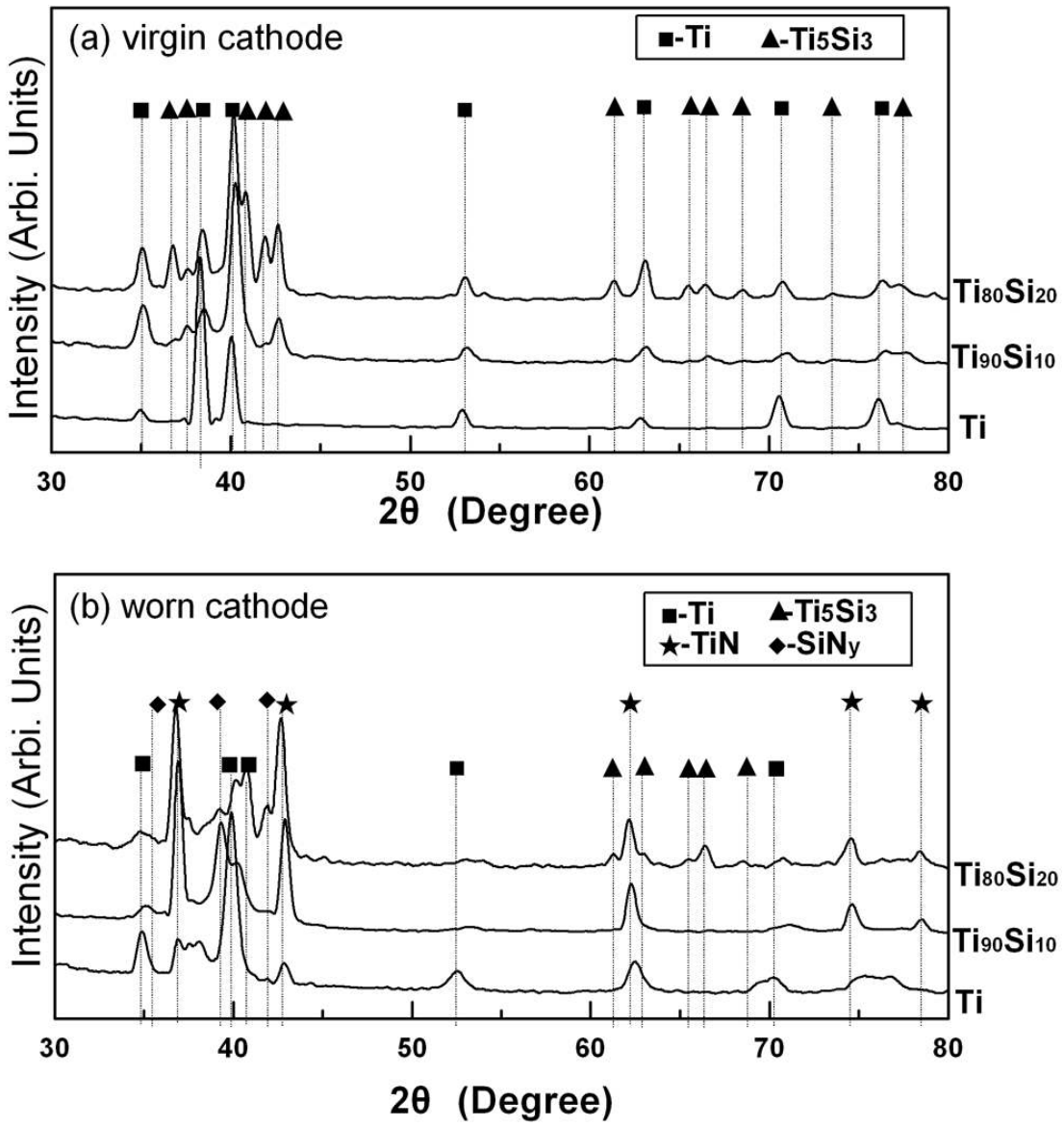

FIG. 1. Grazing-incidence x-ray diffractograms of the cathode surfaces with different Si content: (a) virgin cathode and (b) worn cathode.

Figure 2 shows SEM micrographs of the worn $Ti_{1-x}Si_x$ cathode surfaces for (a) x = 0, (b) x = 0.10, and (c) x = 0.20, respectively. The cathode surfaces are covered with overlapping semi-circular craters with 10-30 μm diameter of resolidified

material that is generated by the moving cathode spot during evaporation. The average crater diameter shows no relation to the composition of the $Ti_{1-x}Si_x$ cathodes. However, the surface roughness of the worn cathodes shows deceasing Ra-values of 8.2 µm, 1.8 µm and 1.6 µm for x = 0.20, x = 0.10, and x = 0, respectively.

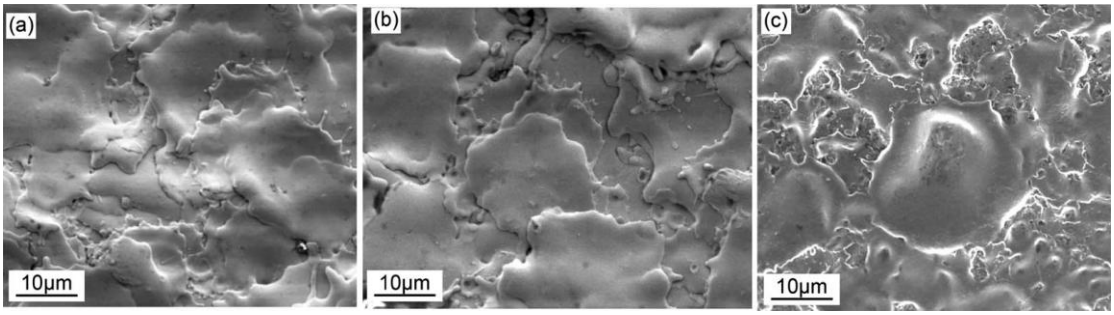

FIG. 2. SEM micrographs of worn cathode surfaces: (a) pure Ti, (b) $Ti_{90}Si_{10,}$ and (c) $Ti_{80}Si_{20}$.

B. Ti cathode worn by reactive cathodic arc evaporation

A cross sectional SEM micrograph of the worn Ti cathode surface is shown in Figure 3. It exhibits a 5 µm to 12 µm thick surface layer on the base Ti material, which microstructure consists of grains several tens of micrometers in size. The undulated top surface is caused by cross section of shallow bowl-shaped craters with a rim.

Figure 4 shows the microstructure and chemical analysis of the worn Ti cathode surface. The cross-sectional STEM overview in figure 4(a) shows that from the initial surface into the interior portion of the cathode, a layer with thickness of approximately 6 µm can be distinguished due to its different grain size compared with the inwards part. The electron diffraction pattern (insert in Figure 4a) of this near surface region shows a mixture of hexagonal α-Ti and fcc-TiN phases, where only

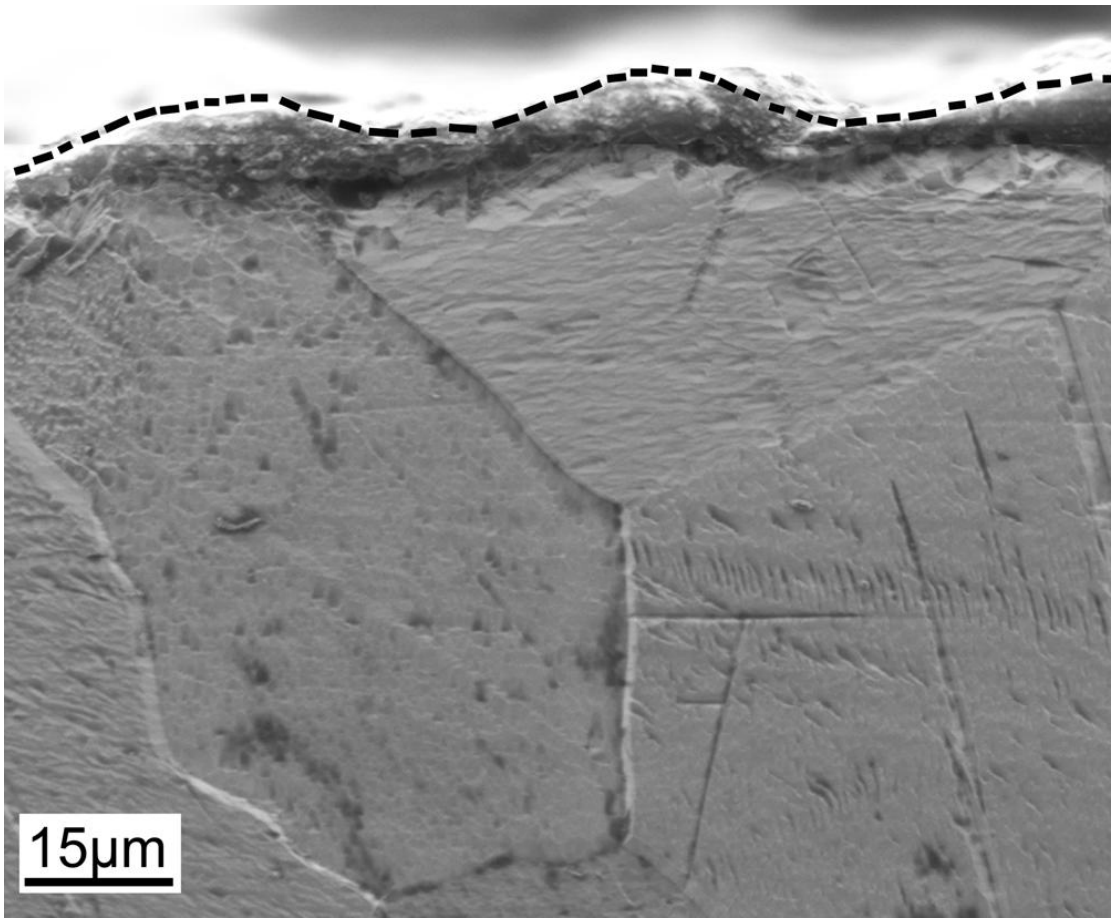

FIG. 3.SEM micrograph of the cross section of the virgin Ti cathode etched to reveal grain structure. The contour of undulation caused by the overlapping craters is indicated by a dashed line.

fcc-TiN is labeled here for distinction. Compared with the continuous rings seen for the α-Ti phase, the TiN phase only displays discrete (111) and (200) diffraction spots. Figure 4b is the in situ measured nitrogen depth profile of the surface layer over the first 7 µm below the surface by EELS with a step size of 10 nm. The white arrow labeled "profile" marks the location of the depth profile. Some grains contain large amounts of N, appearing as deep as 4.5 µm below the surface, while others are N free, i.e. there is no monotonous N-gradient as a function of depth. This appearance is confirmed in the more detailed STEM micrograph and EELS Ti and N elemental

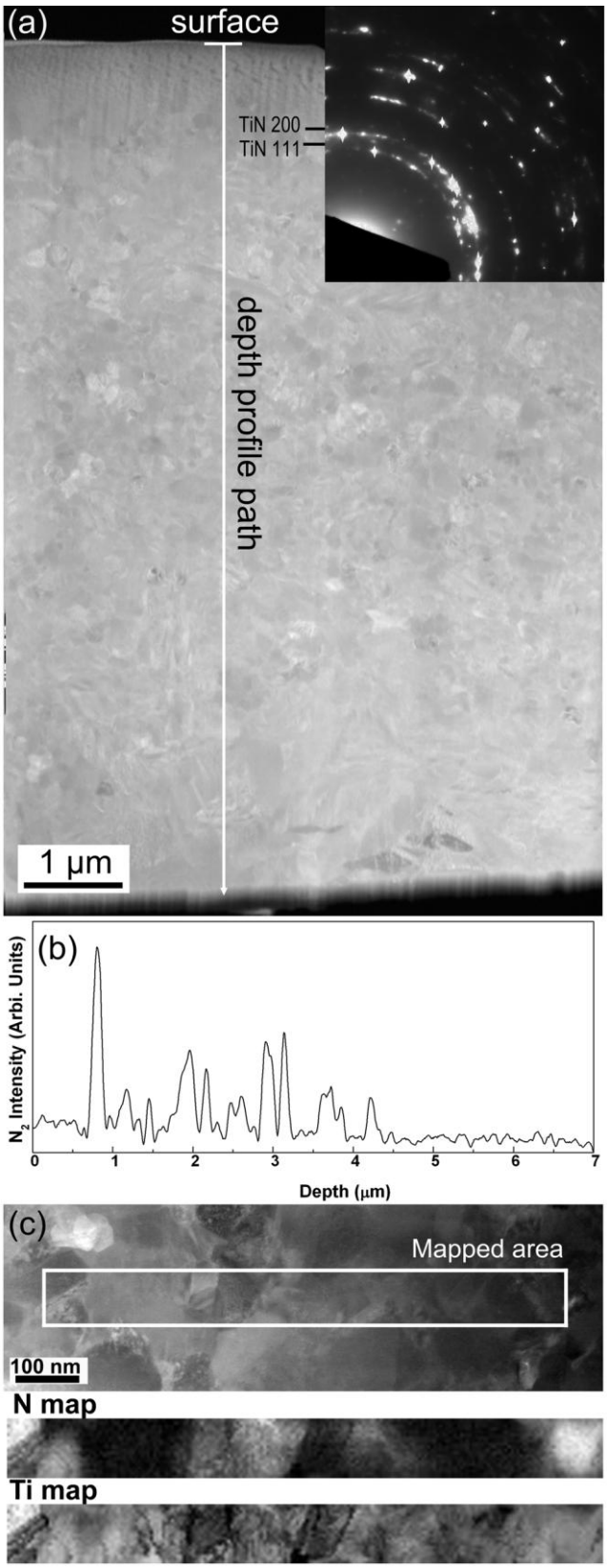

FIG. 4. (a) Cross-sectional STEM micrograph of the converted layer from the top surface of worn Ti cathode with electron diffraction pattern. The curtain feature of the near surface 300 nm region is caused by the FIB milling during sample preparation. (b) EELS N depth profile of the worn Ti cathode surface. (c) STEM micrograph of a selected nanograin region from (a) and EELS maps of N and Ti.

maps in Figure 4(c). The N map shows some grains that are rich in N and others that are free of N. The Ti map shows that all the grains contain Ti. Therefore, the mapped area confirms the depth profile results of selectively nitrided grains and in combination with the XRD results yields the converted layer covering the worn Ti cathode to consist of a mixture of Ti and TiN grains.

C. $Ti_{80}Si_{20}$ cathode worn by reactive cathodic arc evaporation

Figure 5 shows the microstructure and chemical analysis of a cross/section sample from the worn $Ti_{80}Si_{20}$ cathode after reactive CAE from the surface into the unaffected material. A surface converted layer also exists on the cathode surface as can be seen in Figure 5 (a) and (b) of the SEM micrographs. Figure 5(a) shows that the thickness of the converted layer is unevenly distributed across the surface. Its thickness varies in the range of 2-4 μm. Figure 5(b), which is a magnification of the rectangular area in figure 5(a), shows that the layer contains nanosized grains. Figure 5(c) shows a SEM micrograph of a polished and etched cross section from the worn $Ti_{80}Si_{20}$ cathode. The microstructure of the material beneath the layer consists of hexagonally shaped grains surrounded by grains of a fine eutectic microstructure. The EDX-maps in figure 5(d) and 5(e) combined with XRD results indicate that the hexagonally shaped grains are Ti_5Si_3 and the eutectic is a mixture of α-Ti and Ti_5Si_3, consistent with the phase diagram [27-28]. Craters are more commonly observed on top of Ti_5Si_3 grains and hence we conclude that Ti_5Si_3 is preferentially eroded.

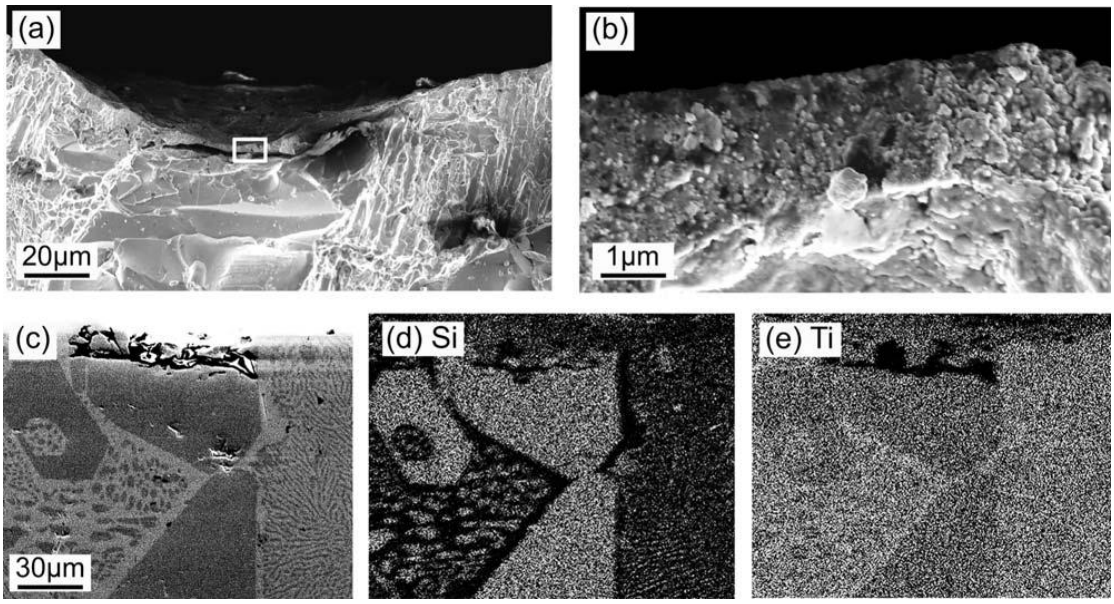

FIG. 5. (a) and (b): cross-sectional SEM micrograph of a worn $Ti_{80}Si_{20}$ specimen prepared by fracturing: (a) low magnification of the cross overview and (b) high magnification micrograph of the compound layer. (c): cross-sectional SEM micrograph of a worn $Ti_{80}Si_{20}$ specimen prepared by chemical etching, and element distribution by using EDX mapping for (d) Si and (e) Ti.

Figure 6 shows the detailed microstructure of the surface layer from the $Ti_{80}Si_{20}$ cathode, including two cross sectional STEM micrographs of the $Ti_{80}Si_{20}$ sample from (a) the rim and (b) the bottom of a crater. Figure 6(a) shows equiaxed nanosized grains of the rim of a crater, which slightly decrease in size at larger depth. The micrograph from the bottom of the crater (Figure 6(b)) shows columnar grains at the surface followed by equiaxed grains. The SAD pattern of the rim region reveals the converted layer to contain three phases, including fcc-TiN phase, hexagonal α-Ti phase and hexagonal Si_3N_4 phase. The converted layer in the crater region has larger grains therefore a lower number of grains are sampled by SAD. Hence, the diffraction pattern contains only a few discrete spots, revealing a mixture of fcc-TiN and α-Ti phases.

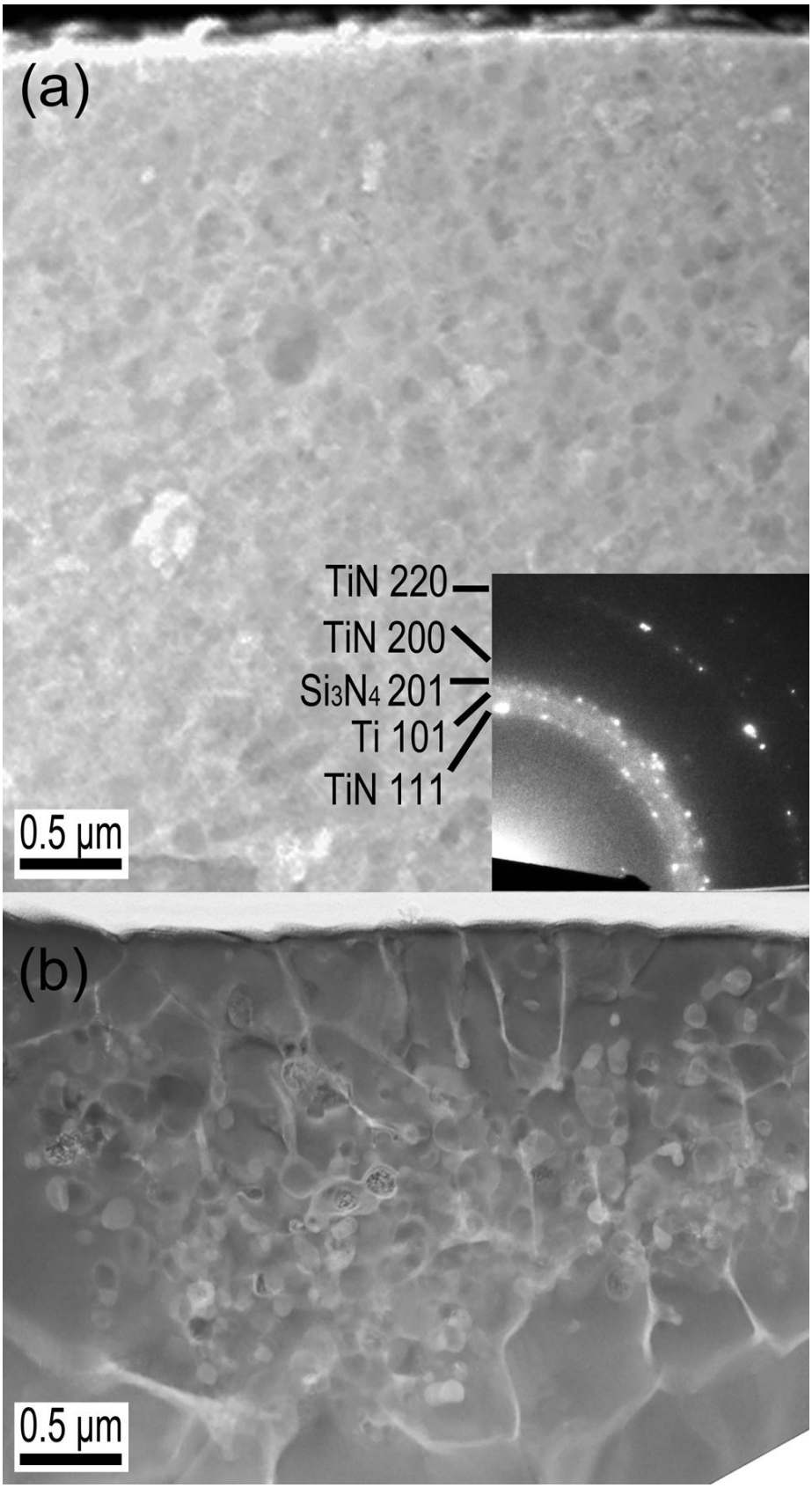

FIG. 6. Cross-sectional STEM micrographs from $Ti_{80}Si_{20}$ cathode: overview image of (a) the rim and (b) the bottom of a crater.

Figure 7 shows EELS elemental maps over an area of 100*100 nm^2 with a pixel resolution of 5 nm from the rim of the crater (seen in Figure 6). The grains are nanocrystalline and either Ti rich or Si rich. The N map shows that the N content is higher in the Ti rich grains than in the Si rich grains.

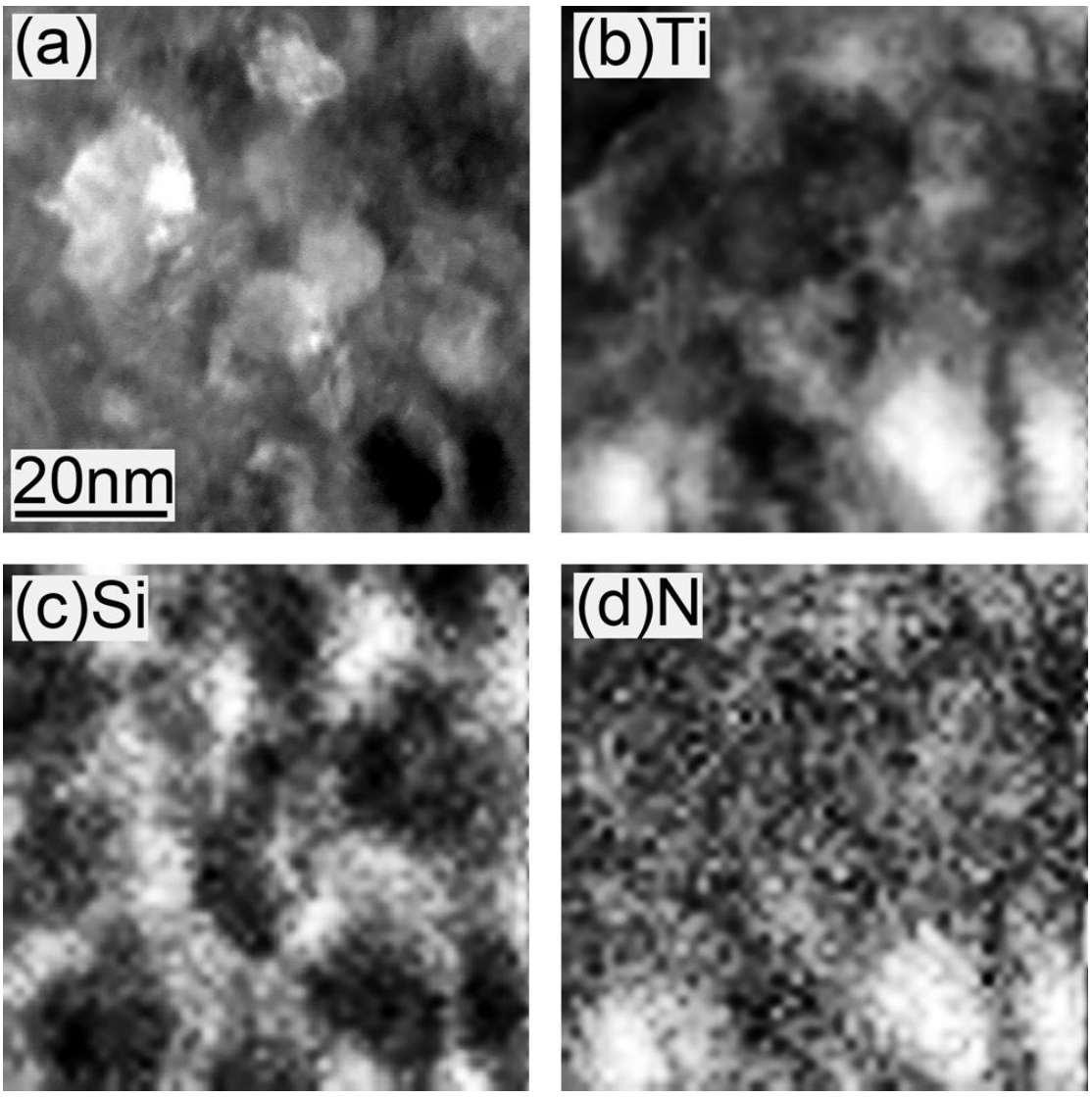

FIG. 7. (a) STEM micrograph from the crater rim of 20% Si-containing cathode, (b) EDX elemental map of Si K_α, (c), and (d) EELS maps of Ti and N.

The EDX elemental maps in figure 8 show the composition distribution at the bottom of a pit from the $Ti_{80}Si_{20}$ cathode. The columnar grains (site 1) contain both Si

and Ti, but they are depleted of Si at the grain boundaries, consistent with Ti_5Si_3 grains with Ti grain boundaries. The equiaxed grains in the converted layer (site 2), have the same features as in the peak region (Figure 7), i.e. Ti or Si rich grains.

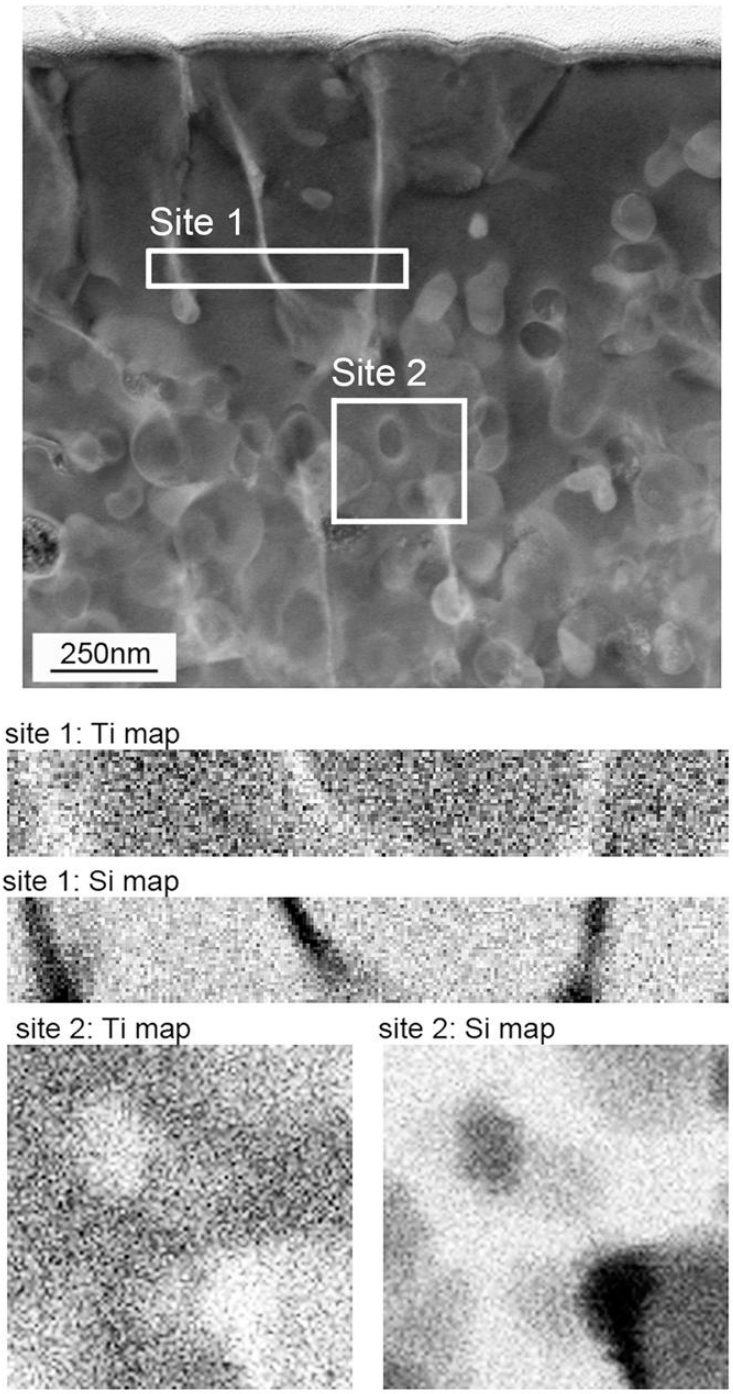

FIG. 8. STEM micrograph of the converted layer from the bottom of the crater of 20% Si containing cathode and EDX elemental maps of site 1: columnar grains; site 2: nanocrystalline grains.

IV. Discussion

The results show that a converted layer forms on the $Ti_{1-x}Si_x$ cathode surfaces during reactive arc evaporation in a N_2 atmosphere. This converted layer ranges from 5-12 μm in thickness for x=0 to 2-4 μm for x=0.2. The surface consists of numerous laterally overlapping craters, which are shallow and bowl-shaped with raised outer rims. They are reported to be caused by the explosive plasma formation and high plasma pressure on the liquid cathode material in the cathode spot [1]. The microstructure and the composition of the converted layer differ with Si content. In the case of pure Ti metal cathodes, the converted layer contains nanocrystalline equiaxed TiN grains dispersed in an α-Ti matrix. In comparison, the microstructure and the composition of the converted layer of the $Ti_{80}Si_{20}$ cathode becomes more complex due to the presence of Si and it additionally contains Si and Si_3N_4. In this case the microstructure also differs between the bottom and the rim of the crater. No Ti_2N phase could be identified by XRD or ED in any of the cathodes, perhaps due to overlapping diffraction lines from Ti and TiN. However, we expect that small amounts of Ti_2N phase exists in the converted layers.

We suggest that the existence of nitrided grains in the converted layer is a result of ejected and buried macroparticles on the surface in the presence of the reactive N_2 gas. During the reactive arc evaporation process, the cathode surface is subject to impingement of N-containing ions, atoms, and molecules at a high rate. The time to form one N-monolayer at the working pressure of 2 Pa N_2 is about 1.5×10^{-4} s. Hence, we infer that the entire cathode surface is continuously covered with N during

the evaporation. Moreover, according to Rosén et al. [29], N^+ ions account for 30% of the entire plasma which is evaporated from a pulsed Zr cathode in the reactive N_2 gas. Similar conditions are expected in this study, e.g., the plasma is rich of activated N^+ ions. As illustrated in figure 9(a), the cathode spots are in a molten state during its lifetime due to the extremely high temperature [30]. The dense plasma in front of the cathode spots generates a high pressure, which exceeds atmospheric pressure by orders of magnitude (0.5 GPa) [31]. The high pressure induces splashes of the molten liquid and macroparticles forms, some of which emit towards the substrate and are embedded in the coatings, while others are redeposited in the vicinity of the crater [32]. Such particles are rapidly cooled and solidify at the crater rim, forming microprotrusions that can serve as new ignition sites. During discharging, activated N^+ ions may nitride these airborne macroparticles in the plasma. The level of nitriding of the macroparticles depends on their dimensions, which range from tens of microns down to a few nanometers in diameter [33]. Most probably, the nanosized particles are more nitrided through continues nitrogen ion bombardment and nitrogen diffusion from the surface into the core while the larger ones are inhomogeneous with a Ti core encapsulated by an outer TiN shell [33]. Further nitriding is expected to take place of the particles when they are redeposited on the cathode surface. The timescale of one discharge event is around a few hundreds nanoseconds [1], while the cathodes in this study were run for 80 min per each deposition. Therefore, the studied cathode surface has reached a cyclic steady-state process of ejecting and redepositing nitrided macroparticles during evaporation and the discrete cathode spots have completely

covered the surface. The cyclic generation of splashes of molten liquid overlayering the nitrided macroparticles eventually forms the converted layer with dispersed N-containing grains. Figure 9(b) schematically illustrates a plan view of the cathode surface after reaching steady state.

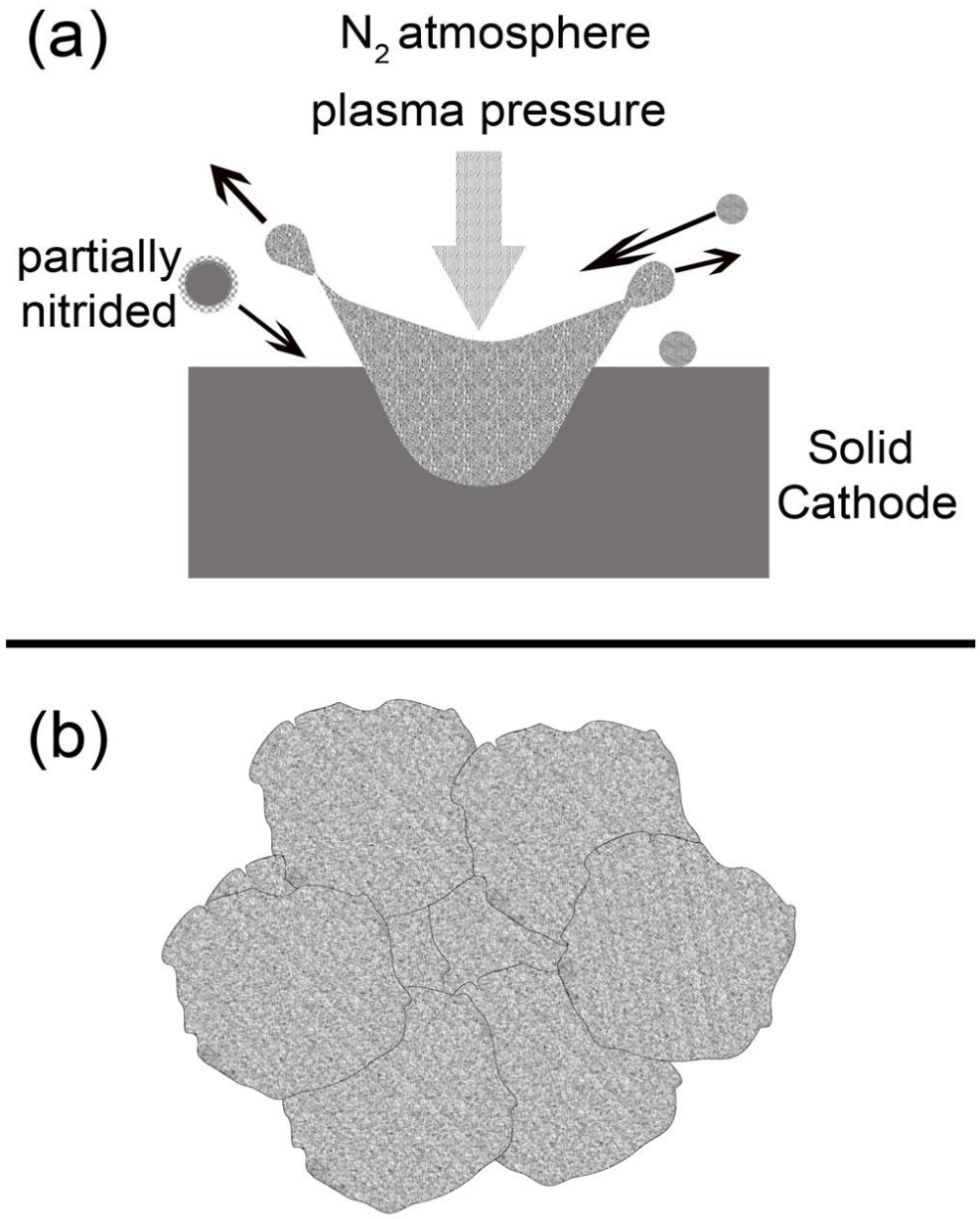

FIG. 9. Schematic illustration of the nitriding mechanism: (a) cross section of a cathode spot; (b) top view of the overlapping cooled cathode spots.

In the case of the Si-containing cathodes, the Ti-Si-N ternary system must be taken into account. According to Sambasivan et al. [28], the general effect of highly activated nitrogen in the Ti-Si-N ternary system is stabilization of compounds and solid solutions of higher silicon contents by producing a nitrided titanium phase. In our case with the extremely high temperature prevailing in the arcing region of the cathode surface, the nitrogen either serves to react with the airborn Ti macroparticles to form TiN phases, or to react with Ti_5Si_3 to form a microstructure with TiN in a Si or Si_3N_4 matrix. The latter also occurs in the regions where a larger fraction of activated N^+ is expected, i.e. at the crater rim.

Arcing introduces a surface roughness from the initially flat cathode surface and the roughness is related to the Si content. The higher roughness seen in cathodes containing 20% Si can be attributed to the preferential erosion of the Ti_5Si_3 phase over surrounding materials. This indicates that the Ti_5Si_3 phase has a different work function to free the electrons compared to the Ti phase. In general, preferential erosion occurs in all multiphase cathodes, which may subsequently influence the composition evolution of the plasma.

Compared to the virgin material, the altered microstructure and compositional features of the converted layer on the cathode surface can be related to the characteristics of the reactive cathodic arc evaporation process, i.e., the drop of the erosion rate of the cathode material. In the case of Ti-Si cathodes, the converted layer has heterogeneous electrical properties compared to the virgin state due to the presence of the reactive arc newly induced TiN and Si_3N_4 phases. The electrical

conductivity of TiN is one order of magnitude less than that of Ti and Si_3N_4 is an insulator. Hence, the converted layer has a complex nature from mixed insulating dieletrical grains relative to the originally conductive Ti grains. The nitrided phases change the electronic structure of the surface as well. The work function of TiN is 0.4 eV lower than Ti [34], which influences the electron emission in a highly nonlinear manner. Thus, the grains of a few hundred nanometers in diameter with altered electrical properties render the arc behavior to be completely different compared to the case of only Ti metallic grains. The insulating nitrided grains may charge under the ion bombardment and build up a stronger electric field. The spot ignition hence occurs more likely on these nitrided grains. Arc interaction with nitrided grains causes a cathode spot of type 1 [1], resulting in a mixture of metal and nitrogen ions as the source to the plasma. In this way, under the condition of a steady state arc current, a fraction of evaporating nitrogen ions from the surface converted layer takes part of the arc current, resulting in the reduction of the cathode material release, i.e., in this way the erosion rate drops compared to the non-reactive evaporation on a pure metal surface.

V. Conclusion

In this work, a combination of FIB and TEM-EELS/EDX characterization methods has enabled the investigation of the microstructural status of the worn Ti-Si cathodes surfaces. The results show that:

- For $Ti_{1-x}Si_x$ cathodes (x=0, x=0.1, and x=0.2), a nitriding multiphase layer forms on the surface when used in a N_2 reactive atmosphere. The converted layer ranges

from 5-12 μm in thickness for x=0 to 2-4 μm for x=0.2 and consists of Ti, TiN, Ti_5Si_3, and Si_3N_4. Therefore, the discharging occurs from a surface that is dynamically different than the virgin material.

- The nitriding mechanism of the converted layer is by a function of the nitrogen reacting with ejecting macroparticles which are subsequently buried in the cathode surface.
- No N-content-gradient appears in the converted layer, instead N-containing grains are formed and dispersed in the layer.
- Selective erosion occurs in two-phase alloyed cathodes, inducing a rougher surface, which also may influence the composition evolution of the plasma.
- Compared to the Ti and Ti_5Si_3 phase in the virgin cathodes, the different electrical properties of the TiN and Si_3N_4 phases formed in the converted layer can be related to the characteristics of reactive cathodic arc evaporation, such as the drop of erosion rate.

VI. Acknowledgements

The funding of this investigation from the VINN Excellence center in Research and Innovation on Functional Nanoscale Materials (FunMat) by the Swedish Governmental Agency for Innovation Systems is gratefully acknowledged. The authors would also like to thank Dr. P. O.Å Persson and J. Palisaitis for their help with EELS.

VII. Reference

1. A. Anders, *cathodic Arc*. (Springer, 2008).

2. I. J. Smith, W. D. Münz, L. A. Donohue, I. Petrov and J. E. Greene, Surface Engineering **14** (1), 37-41 (1998).

3. J. G. Han, J. S. Yoon, G. E. Kim and K. Song, Surface & coatings technology **86-87**, 82-87 (1996).

4. Y. Tanaka, T. M. Gür, M. Kelly, S. B. Hagstrom and T. Ikeda, Thin Solid Films **228** (1-2), 238-241 (1993).

5. M. Oden, L. Rogstrom, A. Knutsson, M. R. Terner, P. Hedstrom, J. Almer and J. Ilavsky, Applied Physics Letters **94** (5), 053114-053113 (2009).

6. A. Knutsson, M. P. Johansson, P. O. A. Persson, L. Hultman and M. Oden, Applied Physics Letters **93** (14), 143110-143113 (2008).

7. A. Hörling, L. Hultman, M. Odén, J. Sjölen and L. Karlsson, Surface and Coatings Technology **191** (2-3), 384-392 (2005).

8. P. Holubar, M. Jilek and M. Sima, Surface and Coatings Technology **120-121**, 184-188 (1999).

9. J. Almer, M. Oden and G. Hakansson, Thin Solid Films **385** (1-2), 190-197 (2001).

10. M. Odén, J. Almer and G. Hakansson, Surface & Coatings Technology **121**, 272-276 (1999).

11. J. Rosén, A. Anders, L. Hultman and J. M. Schneider, Journal of Applied Physics **94** (3), 1414-1419 (2003).

12. F. Richter, G. Krannich, M. Kuhn, S. Peter and C. Spaeth, Trends and New Applications of Thin Films **287-2**, 193-197 (1998).

13. B. F. Coll and D. M. Sanders, Surface & Coatings Technology **81** (1), 42-51 (1996).

14. G. E. Kim, J. L. Meunier and F. Ajersch, IEEE Transactions on Plasma Science **23** (6), 1001-1005 (1995).

15. R. L. Boxman and S. Goldsmith, Surface & Coatings Technology **33** (1-4), 153-167 (1987).

16. B. F. Coll and M. Chhowalla, Surface & Coatings Technology **68**, 131-140 (1994).

17. I. I. Aksenov, I. I. Konovalov, V. F. Pershin, V. M. Khoroshikh and L. F. Shpilinskii, High Temperature **26** (3), 315-318 (1988).

18. M. Kuhn and F. Richter, Surface & Coatings Technology **89** (1-2), 16-23 (1997).

19. D. P. P. Hovsepian, J. Vacuum **45** (5), 603-607 (1994).

20. H. Söderberg, M. Odén, T. Larsson, L. Hultman and J. M. Molina-Aldareguia, Applied Physics Letters **88** (19) (2006).

21. L. Hultman, J. Bareno, A. Flink, H. Söderberg, K. Larsson, V. Petrova, M. Odén, J. E. Greene and I. Petrov, Physical Review B. **75** (15) (2007).

22. H. Ljungcrantz, M. Odén, L. Hultman, J. E. Greene and J. E. Sundgren, Journal of Applied Physics **80** (12), 6725-6733 (1996).

23. M. Odén, H. Ljungcrantz and L. Hultman, Journal of Materials Research **12** (8), 2134-2142 (1997).

24. L. Hultman, C. Engstrom, J. Birch, M. P. Johansson, M. Odén, L. Karlsson and H. Ljungcrantz, Zeitschrift Fur Metallkunde **90** (10), 803-813 (1999).

25. S. Sambasivan, W.T. Petuskey., J. Mater. Res. **9**, 2362-2369 (1994).

26. R. M. Langford and A. K. Petford-Long, J. Vac. Sci. Technol. A **19**, 2186-2193 (2001).

27. M. Hansen, H. D. Kessler and D. J. Mcpherson, Trans. ASM. **44**, 518-538 (1952).

28. S. Sambasivan and W. T. Petuskey, J. Mater. Res. **9**, 2362-2369 (1994).

29. J. Rosén, A. Anders, L. Hultman and J. M. Schneider, Journal of Applied Physics **96** (9), 4793-4799 (2004).

30. B. Juttner, J. Phys. D **30**, 221-229 (1997).

31. B. Juttner, In Beitrage aus der plasmaphysiks **19**, 25 (1979).

32. A. W. Baouchi and A. J. Perry, Surface & Coatings Technology **49** (1-3), 253-257 (1991).

33. H. Ljungcrantz, L. Hultman, J. E. Sundgren, G. Hakansson and L. Karlsson, Surface & Coatings Technology **63** (2), 123-128 (1994).

34. S. Yamamoto, The Journal of Chemical Physics **60** (10), 4076-4080 (1974).